RECENT ADVANCES IN FLUID MECHANICS
Proceedings of the Fourth International Conference on Fluid Mechanics, July 20~23, 2004, Dalian, China

ADAPTIVE OPTIMAL CONTROL OF THE INCOMPRESSIBLE FLOW AROUND AN AIRFOIL WITH SMART SURFACE*

Chuijie Wu [1,2,3], *Liang Wang* [2]

[1] *LNM, Institute of Mechanics, Chinese Academy of Sciences, Beijing, 100080, China*
[2] *Research Center for Fluid Dynamics, PLA University of Science and Technology, Nanjing 211101, China*
[3] *State Key Laboratory for Turbulence Research, Peking University, Beijing 100871, China*
Email: cjwu@mech.pku.edu.cn

Abstract: In this paper, using the moving boundary CFD method, we developed a new real-time optimal control method which can adaptively change the shapes of body surface to obtain the unsteady optimal airfoil. The results show that the aerodynamics properties of airfoil with the new method can be improved remarkably, and the aerodynamics characteristics of the final optimal airfoil at different angles of attack are all superior than the original airfoil NACA0012.
Keywords: optimal control with smart surface, unsteady separated flow, moving boundary CFD method

1. INTRODUCTION

The Nature creates millions of strange creatures during the billions years of evolution, and every day these living things moves around the world in their graceful, unique and the most energy saving way. But up to now, we are still aware of very little on the mechanism of fluid mechanics of various unsteady boundary motion, such as the moving body surface, associated with the locomotion of these creatures. We hope to increase our understanding of the inscrutability by means of studying the unsteady optimal control of the adaptive smart surface in complex flows.

On the other hand, now in the community of fluid mechanics, the unsteady control and compliant surface technique are becoming the most compelling research directions. The rapid development of MEMS, MAFC and smart materials, such as the shape memory alloy, make the dreams to become true.

In this paper, we developed a new real-time optimal control method which can adaptively change the shapes of body surface to obtain the unsteady optimal airfoil. This study is not only important for the dynamical stall of airfoils, and will boost the experiments and manufactures of smart surfaces and artificial muscles, and also will provide new theories and concepts for the optimal designs, biological locomotion (such as fish swimming) and other control methods.

2. NUMERICAL METHOD AND THE ALGORITHM OF OPTIMAL CONTROL

2.1 Numerical method

The 2D incompressible integral form Navier-Stokes and continuity equations

$$\left.\begin{aligned} &\frac{\partial}{\partial t}\int_\Omega \rho u_i \mathrm{d}\Omega + \int_S \rho u_i \boldsymbol{v}\cdot\boldsymbol{n}\mathrm{d}S = \int_S \tau_{ij}\boldsymbol{i}_j\cdot\boldsymbol{n}\mathrm{d}S - \int_S p\boldsymbol{i}_i\cdot\boldsymbol{n}\mathrm{d}S + \int_\Omega(\rho-\rho_0)g_i\mathrm{d}\Omega \\ &\int_S \rho\boldsymbol{v}\cdot\boldsymbol{n}\mathrm{d}S = 0 \end{aligned}\right\} \quad (1)$$

are solved by finite volume scheme[1] on C type grids.

* The project supported by the National Natural Science Foundation of China (.10172095) and LNM, Institute of Mechanics, CAS.

The second order implicit three time level scheme is used for integration in time. This leads to the following approximation of the unsteady term

$$\left[\frac{\partial}{\partial t}\int_{\Omega}\rho u_i \mathrm{d}\Omega\right]_P \approx \frac{\rho\Delta\Omega}{2\Delta t}(3u_i^{n+1}-4u_i^n+u_i^{n-1}) = A_P^t u_{i,P}^{n+1} - Q_{u_i}^t \tag{2}$$

where

$$A_P^t = \frac{3\rho\Delta\Omega}{2\Delta t}, \qquad Q_{u_i}^t = \frac{\rho\Delta\Omega}{2\Delta t}(4u_i^n+u_i^{n-1}) \tag{3}$$

The surface integrals may be split into four control volume(CV) face integrals which can be approximated by the midpoint rule. So $\int_S f\,\mathrm{d}S = \sum_c \int_{S_c} f\,\mathrm{d}S = \sum_c \overline{f}_c S_c \approx \sum_c f_c S_c, c = e,w,n,s$, where $\overline{f}_c$ is the mean value of the integrand over the face 'c' and f_c is the value of the integrand at the face center. The approximation of the volume integral is

$$\int_{\Omega} g\,\mathrm{d}\Omega \approx g_P\Delta\Omega \tag{4}$$

where g_p is the value of the integrand at the CV center P.

2.2 The conservation problem in the moving grid system

When the cell faces move, the conservation of mass(and all other conserved quantities) is not necessarily ensured if the grid velocities are used to calculate the mass fluxes. Mass conservation can be obtained by enforcing the so-called space conservation law (SCL) which can be thought of as the continuity equation for zero fluid velocity:

$$\frac{\mathrm{d}}{\mathrm{d}t}\int_{\Omega}\mathrm{d}\Omega - \int_S \boldsymbol{v}_b\cdot\boldsymbol{n}\,\mathrm{d}S = 0 \tag{5}$$

This equation describes the conservation of space when the CV changes its shape and/or position with time. Eq.(5) reads, in discretized form $\frac{(\Delta\Omega)^{n+1}-(\Delta\Omega)^n}{\Delta t} = \sum_c (\boldsymbol{v}_b\cdot\boldsymbol{n})_c S_c$, where $c = e,w,n,s$.

The difference between the 'new' and the 'old' CV volume can be expressed as the sum of volume $\delta\Omega_c$ swept by the CV faces during the time step.

$$\frac{(\Delta\Omega)^{n+1}-(\Delta\Omega)^n}{\Delta t} = \frac{\sum_C \delta\Omega_C}{\Delta t} \tag{6}$$

By comparing these two equations, we see that the volume swept by one cell face is $\dot{\Omega}_c = (\boldsymbol{v}_b\cdot\boldsymbol{n})_c S_c = \frac{\delta\Omega_c}{\Delta t}$. The mass flux through a cell face 'c' can be calculated as $\dot{m}_c = \int_{S_c}\rho(\boldsymbol{v}-\boldsymbol{v}_b)\cdot\boldsymbol{n}\,\mathrm{d}S \approx \rho_c(\boldsymbol{v}\cdot\boldsymbol{n})_c S_c - \rho_c\dot{\Omega}_c$. For the implicit Euler scheme, the discretized continuity equation reads $\frac{(\rho\Delta\Omega)^{n+1}-(\rho\Delta\Omega)^n}{\Delta t} + \sum_c \dot{m}_c = 0$, where $c = e,w,n,s$. The unsteady term has to be treated in a way that is consistent with the space conservation law. For incompressible flows, the contribution of the grid movement to the mass fluxes has to cancel the unsteady term, i.e. the mass conservation equation reduces to $\int_S \rho\boldsymbol{v}\cdot\boldsymbol{n}\mathrm{d}S = 0$. Then the mass conservation law is satisfied in the moving grid system.

2.3 The optimal method

The optimal method that we used is an approach to nonlinearly constrained minimal problems[2]. The problem we consider is the following. Let m_1, m_2, m_3 be integers with $0 \le m_1 \le m_2 \le m_3$, let f_i be given real numbers and let g_i be given smooth functions. We wish to choose $x_1, \cdots, x_n$ to

$$\left.\begin{array}{ll} \min \omega & \\ |f_i - g_i(x_1,\cdots,x_n)| \le \omega & 1 \le i \le m_1 \\ g_i(x_1,\cdots,x_n) \le \omega & m_1+1 \le i \le m_2 \\ g_i(x_1,\cdots,x_n) \le 0 & m_2+1 \le i \le m_3 \end{array}\right\} \tag{7}$$

To implement the optimal method to unsteady optimal control, the first task is to find a parameter space for a large range of airfoil shapes. Chang et al.[3] introduced a parameter space suitable for our current purpose. An airfoil can be defined by up to 20 parameters and supercritical airfoils are included in this space.

3. THE PROCEDURE OF UNSTEADY OPTIMAL CONTROL

The procedure of unsteady optimal control is as follows: (1) Parameterizing the original airfoil to get the initial parameters $\boldsymbol{x}_0$; (2) Using the original airfoil to create the initial grid; (3) Computing the flow field on the initial grid till t_0 at which the process of control start; (4) Saving the shape of airfoil and C_l^0, C_d^0 at t_0. Calculating the value of the objective function $J(\boldsymbol{x}_0)$; (5) Finding a search step $\boldsymbol{h}$ and reconstructing the new airfoil using $\boldsymbol{x}_0+\boldsymbol{h}$; (6) Creating new grid by using the new airfoil. Then, interpolating the flow field at t_0 into the new grid to get the new initial field. (7) Using the new grid and the new initial field to compute the flow field at t_0+dt (dt is the time step) and the value of objective function $J(\boldsymbol{x}_0+\boldsymbol{h})$; (8) If $J(\boldsymbol{x}_0+\boldsymbol{h})<J(\boldsymbol{x}_0)$ and all of the constrains are satisfied, we will let $\boldsymbol{x}_0=\boldsymbol{x}_0+\boldsymbol{h}$, and $J(\boldsymbol{x}_0)=J(\boldsymbol{x}_0+\boldsymbol{h})$; (9) The process of optimal will be stop if the value of objective function cannot be reduced anymore and the process of (5)~(8) will be repeated otherwise. (10) Computing the flow field on the new grid corresponding to the optimized airfoil till $t_0+\Delta t(\Delta t \gg \mathrm{d}t)$ at which the next control start; (11) The program will be stop if the terminal condition is satisfied and let $t_0=t_0+\Delta t$, then repeat (4)~(10) otherwise.

4. NUMERICAL RESULTS

4.1 Controlling the airfoil at fixed attack angle

The initial airfoil NACA0012 should be parameterized at first. The following special shape functions are used

$$\left.\begin{array}{l} g_1(x)=\sqrt{x}-x, \quad g_2(x)=x(1-x), \quad g_3(x)=x^2(1-x) \\ g_4(x)=x^3(1-x), \quad g_5(x)=x^4(1-x) \end{array}\right\} \tag{8}$$

Both the upper and the lower surfaces are defined by these five shape functions. So the dimensions of our parameter space is 10.

We use C type grid of total 240×40 at Re_c=1 000 and α=12°. The objective function is

$$J(\boldsymbol{x})=|C_l-0.6|+\frac{C_d}{C_d^0} \tag{9}$$

where $\boldsymbol{x}$ is the vector of parameters which is to be optimized and 0.6 is the result of analyzing the lift coefficient of NACA0012 at Re_c=1 000 and α=12°. The average lift coefficient in that condition is about 0.48. To increase the lift at the same time of decreasing the drag, we choose the moderate value as the object of lift.

All of our constrains are geometry constrains. The geometry constrains can be added without any additional running of flow solver. What we choose are: (1) The airfoil thickness is limited to 12% chord length; (2) The camber is limited to 2% chord length; (3) The leading edge radius is controlled by the distance between the two points which are adjacent to the leading edge point on the upper and lower surface. The limitation of this distance is set to 0.4% chord length; (4) The limitation of the maximum

distance between the two optimal airfoil which are adjacent to each other is set to 0.5% chord length.
The original and the optimal airfoils in the process of unsteady optimal control are shown in Fig.1. We can see that the difference between the two optimal airfoils which are adjacent to each other is smaller and smaller, and finally, the shape of the optimal airfoil is almost fixed.
The two airfoils shown in Fig.2 are NACA0012 and the optimal airfoil at t=15. The maximum thickness of the optimal airfoil is 11.11% chord length; The maximum camber is 1.97% chord length; The leading edge radius is 0.496% chord length. All of our constrains are satisfied and all of the maximum geometrical parameters are very closed to their limitation. That is why the shape of the optimal airfoils is almost fixed at last.

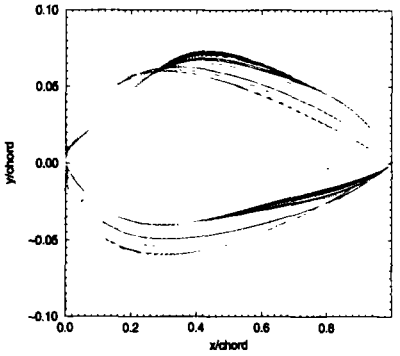

Fig.1 NACA0012 and the optimal airfoils

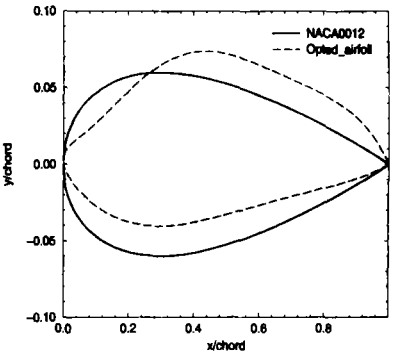

Fig.2 NACA0012 and the final optimal airfoils(t=15)

Figure 3(a) is the history of L/D of NACA0012 and the unsteady optimal airfoil. The total computational time is 15, and the control is introduced in at t=1.5. The control interval time is $\Delta t = 0.05$. From the figure, it can be seen that the L/D oscillates a lot before t=2.0, and they are correspond to the big changes of the shape of the airfoil, as shown in Fig.1. After t>2.0, due to the limit of constrains, the shape changes smaller and make the optimal airfoil converges to a final state, therefore the amplitude of oscillation of the corresponding L/D decreases and becomes much smaller than the one of NACA0012. The final L/D increases from 3.827 to 5.001, which is 30.8% higher than the original one.
Figure 3(b) and Fig.3(c) are the time history of the lift and drag coefficients of NACA0012 and the unsteady optimal airfoil, respectively. From Fig.3(b), one can see that after the optimal airfoil reaches the final shape, the average of lift coefficient increases from 0.481 to 0.602, or 25.3% larger, and from Fig.3(c), the average drag is reduced about 4.1% (from 0.125 drops to 0.120).

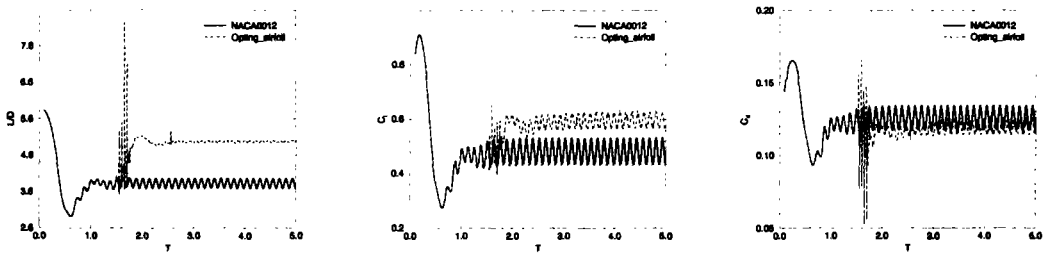

(a) the history of L/D (b) the history of C_l (c) the history of C_d

Fig.3 Aerodynamics parameter of NACA0012 and the optimal airfoils

In addition, we calculate the aerodynamics parameters of the optimal airfoil in Fig.2 at α=12° and α=14° when Re_c=1 000 and which at Re_c=2 000, Re_c=3 333 and Re_c=5 000 when α=12°. The results are listed in Table 1.

Table 1 Comparison of $\overline{C_l}$, $\overline{C_d}$ and $\overline{L/D}$ at variant attack angle and Reynolds number

Re_c	$\alpha(^\circ)$	NACA0012			Optimal airfoil (t=15)			Increasment(%)		
		$\overline{C_l}$	$\overline{C_d}$	$\overline{L/D}$	$\overline{C_l}$	$\overline{C_d}$	$\overline{L/D}$	$\Delta\overline{C_l}$	$\Delta\overline{C_d}$	$\Delta\overline{L/D}$
1 000	10	0.397	0.093	4.287	0.505	0.084	6.035	27.363	-9.507	40.778
1 000	12	0.481	0.125	3.827	0.606	0.120	5.030	26.068	-3.973	31.428
1 000	14	0.587	0.172	3.405	0.700	0.170	4.103	19.191	-0.738	20.474
2 000	12	0.482	0.132	3.619	0.712	0.149	4.773	47.658	12.524	31.879
3 333	12	0.580	0.153	3.761	0.811	0.179	4.506	39.969	16.994	19.826
5 000	12	0.868	0.194	4.440	0.868	0.181	4.774	-0.053	-6.743	7.541

4.2 Optimal control of an oscillating airfoil

We take NACA0012 again as the starting airfoil and solve the flow on C type grid (240×40) at Re_c=1 000. The oscillating rule is $\alpha=\alpha_0+3^\circ\sin(\omega t)$, where $\alpha_0=9^\circ$; The period of oscillation is T=1.0. The objective function is

$$J(\boldsymbol{x})=|C_l-C_l^0|/C_l^0+20C_d/C_d^0 \tag{10}$$

The total time of optimal control is 10.0, and the control starts at t=2.0 with the control interval equals to $\Delta t=0.05$. Figure 4 shows the time history of the optimal airfoil. Figure 5 and Fig.6 are the time histories of the aerodynamics coefficients of the pitching motions of NACA0012, unsteady optimal airfoil and the fixed shape optimal airfoil(the shape of the airfoil is obtained at t=10), respectively. From the figures, we

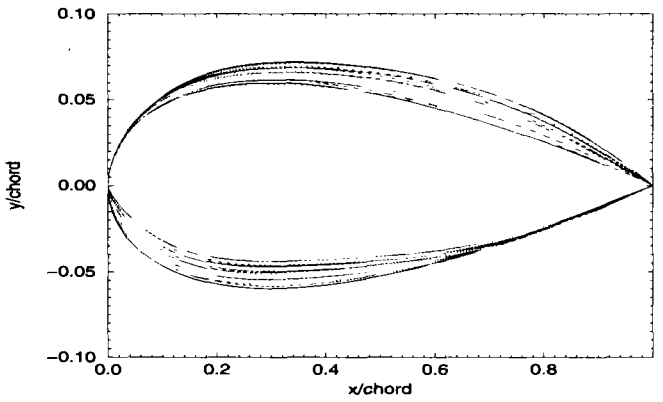

Fig.4 NACA0012 and the optimal airfoils in the pitching motion

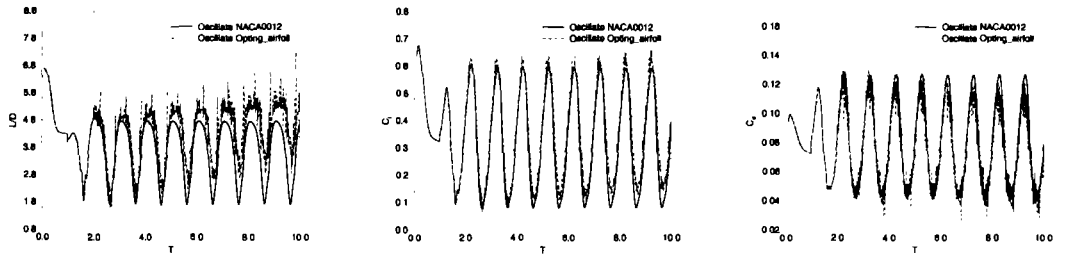

(a) the history of L/D (b) the history of C_l (c) the history of C_d

Fig.5 Aerodynamics parameter of NACA0012 and the optimal airfoils in the pitching motion

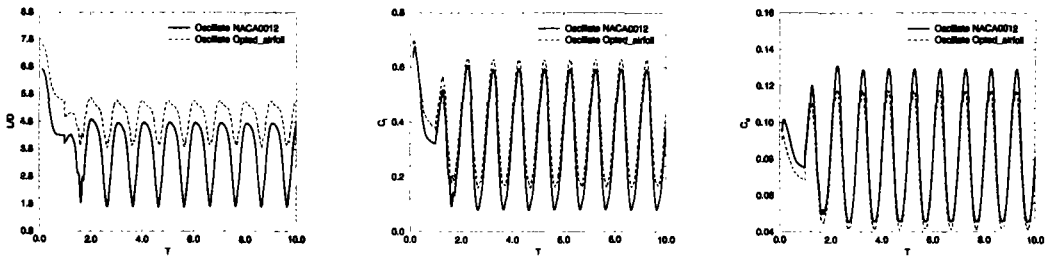

(a) the history of L/D (b) the history of C_l (c) the history of C_d

Fig.6 Aerodynamics parameter of NACA0012 and the final optimal airfoils (t=10)

can find that the aerodynamics properties are improved, and even the properties of hysteresis loops of the unsteady optimal airfoil are better than the one of NACA0012, as shown in Fig.7.

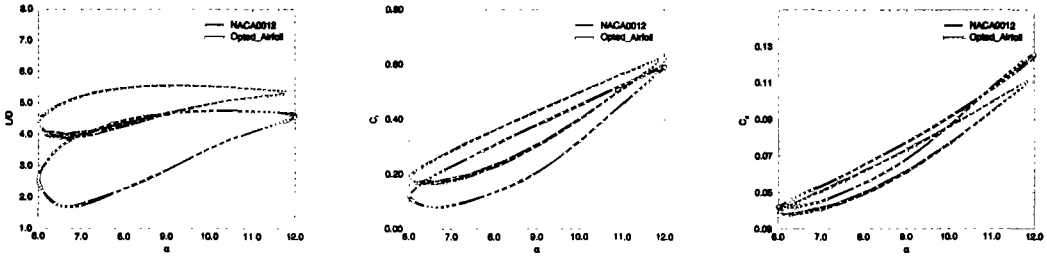

(a) the history of L/D (b) the history of C_l (c) the history of C_d

Fig.7 Hysteresis loops comparison of the original airfoil and the final optimal airfoil

5. CONCLUSION

From above, one can conclude that: (1) Using the method of optimal control, the aerodynamics properties of airfoil can be improved remarkably; (2) With certain geometrical constrains, the optimal airfoil will be converged at last; (3) The aerodynamics characteristics of the final optimal airfoil at different angles of attack are all superior than the original airfoil NACA0012; (4) The adaptive smart airfoil always performs optimally under different flight conditions; (5) Even we did not aim at improving the hysteresis loop properties of the pitching motion of airfoil, but the results show that the unsteady optimal airfoil has better performs in the pitching motion.

REFERENCES

1. Ferziger J H, Perić M. Computational Method for Fluid Dynamics. Spinger, 1999
2. Kaufman EK, Leeming DJ, Taylor GD. An ODE-based approach to nonlinearly constrained minimax problems. *Numerical Algorithms*, 1995, 9: 25~37
3. Chang IC, Torres FJ, Tung C. Geometric Analysis of Wing Sections, NASA Technical Memorandum 110346, 1995